First-principles investigations of electronic and optical properties of Er-doped GaN involved in ErGaN/ErN quantum well heterostructures

S. Amiri[a], K. Agroui[b], B. Amiri[c], M. Abboun Abid[d], and A. Belghachi[e]

[a]Department of Electrical Engineering, Laboratory Simulation, Commanded, Analysis and Maintenance Electrical Network,
National Polytechnic School of Oran-Maurice Audin, BP 1523 El Mnaouer, Oran, Algeria.
[b]Semiconductors Technology for Energetic Research Center (CRTSE) BP 140 Alger-7 Merveilles Algeria.
[c]Higher Normal School of Bechar, Algeria.
[d]National Polytechnic School of Oran-Maurice Audin, BP 1523 El Mnaouer, Oran, Algeria.
[e]Bechar university Tahri Mohamed, BP 417 Bechar, Algeria.

We study the electronic, the optical and the transport properties of both bulk materials ErN and $Er_{0.125}Ga_{0.875}N$, which crystallize in zinc-blind and wurtzite structures, respectively, and are utilized in quantum well devices. The properties are calculated using density functional theory (DFT), by applying the full-potential linearized augmented plane-wave (FP-LAPW) method with a spin-orbit coupling effect. The analysis of the electronic properties shows that ErN and $Er_{0.125}Ga_{0.875}N$ have a band gap at 0.79 and 3.38 eV, respectively. On the other hand, the technology makes it possible to stack these materials for a quantum well heterostructure of $Er_{0.125}Ga_{0.875}N/ErN$. The optical properties such as optical coefficients, refractive index and extinction coefficient are discussed in detail. The transport properties of alloys are investigated using the semi-classical Boltzmann theory as implemented in the BoltzTraP code in conjunction with ab initio electronic structure calculations. Our findings suggest that Er doping of wide band gap semiconductors could be a viable option for quantum well devices.

Keywords: RE:III−N quantum well GGA+U BoltzTrap.

1. Introduction

Semiconductors are used in the vast majority of modern electronic devices. As a result, plenty of research is being conducted to improve their electronic and optical properties with this ever-increasing number of available materials; it is becoming increasingly important to predict the optical properties of new materials in order to determine their usability in optoelectronic devices such as semiconductor lasers or solar cells [1]. $III−N$ compounds are direct band gap energy (E_g) ranging from 0.7 eV for InN, 3.42 eV for GaN, and 6.2 eV for AlN. They can be used at high-temperature, high-frequency, and high-power microelectronic devices. In particular, the GaN is an excellent compound, due to its thermal stability, high thermal conductivity, strong bonding, and distinguished structural, physic-chemical properties [2]. Of particular importance from theoretical and experimental viewpoints, BBiN and Gd doped $III−N$ have been studied in detail by Sam *et al.*, and Amiri *et al.*, respectively [3, 4]. These materials hold enormous promise in optoelectronic and spintronic applications. The electronic configuration of each lanthanide RE element is often denoted as $[Xe]4f^n$, where $[Xe]$ is the electronic configuration of xenon and n is the number of electrons in the inner $4f$ shell. When incorporated into a host material, the RE atom tends to form a trivalent ion (RE^{3+}). An interesting aspect of these compounds is the occurrence of localized strongly correlated $4f$ electrons, the treatment of which presents a challenge to band-structure theory [5]. The incorporation of rare-earth elements into $III−N$

is of significant interest for different industrial applications because of their temperature independence and stable emission together with the possibility of optical or electrical excitation [6, 7]. Rare-Earth elements doped $III−V$ are arguably among of the most studied in optical-electronic devices using principles of band gap engineering and quantum confinement. Their applications spanning from a laser, light-emitting diode (LED), vertical-cavity surface-emitting lasers (VCSELs), and quantum-confined Stark effect (QCSE) [8]. The cause of energy loss by transmission or thermalization of photons is related to the shift between the incident solar spectrum and the band gap of most solar cells. The photon conversion strategies such as downconversion, upconversion, and downshifting are possible technologies to increase the efficiency of solar cells. In this regard, trivalent lanthanide ion-doped luminescent materials have attracted great interest due to their promising application as spectral converters [9–11]. Er-doped $III−N$ materials have been investigated using different growth methods such as ion implantation; Steckl *et al.* [12] have reported on the fabrication of GaN-based display materials doped with various high concentrations of rare-earth ions and have fabricated electroluminescent devices by molecular beam epitaxy (MBE). Altahtamouni *et al.* [13], have synthesized Er-doped GaN quantum well structures by metal organic chemical vapor deposition (MOCVD) [13]. This was the motivation for the theoretical study of electronic, optic, and transport properties of both bulk materials heterostructure ErGaN/ErN where the barrier and well crystallize in wurtzite and zinc-blind structure, respectively. Our

calculations are based on the GGA+U method with a spin-orbit coupling effect. The structural band, optical parameters, and transport properties are calculated. The rest of the paper is organized as follows: Section 2 provides a brief overview of the computational method used. The detailed electronic properties are discussed in Sec. 3.1. Section 3.2 goes over the optical properties and 3.3 discusses transport properties. Finally, Sec. 4 concludes the paper.

2. Computational details

We have investigated the electronic, optical and transport properties of ErN and ErGaN bulk materials shown in Fig. 1, based on DFT [14, 15] using the FP-LAPW method [16, 17] as implemented in the Wien2k code [18]. To calculate the exchange correlation potential, the GGA+U approach was utilized with a spin-orbit coupling effect, we have used the
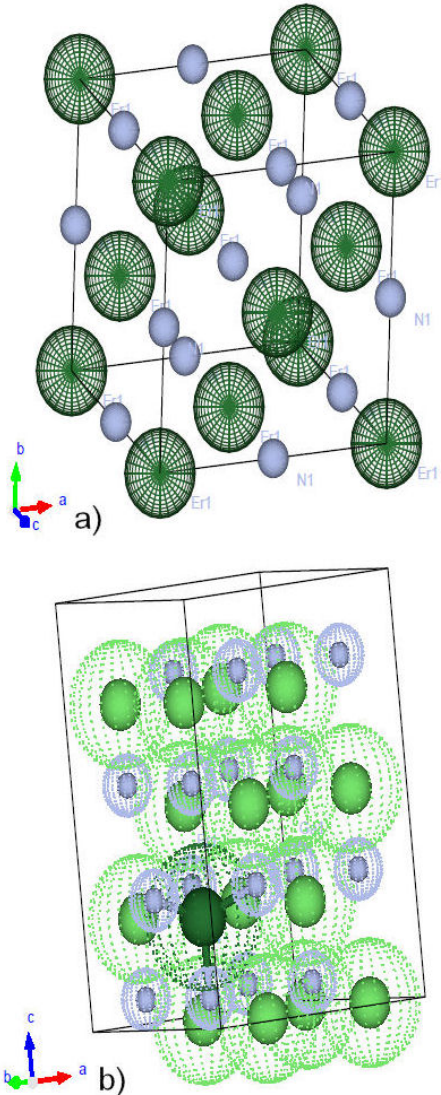
Hubbard potential $U = 8$ eV and $J = 0$ eV for $4f$ electrons of Er as already reported by Harmon *et al*. [19], and modified Becke-Jonson approximation (mBJ) [20]. The wurtzite structure of GaN contains 16 atoms, 8 atoms of Ga and 8 atoms of N, one atom of Ga was substituted by one Er atom, to obtain the ErGaN corresponding to a doping concentration 0.125 % of Er. The wave functions are expanded into planes waves in the interstitial region with a cut-off $K_{\max} = 8/RMT$ where RMT has the smallest of all MT sphere radii and $K_{\max}$ is the plane wave cut-off structures ErN and ErGaN we used 2000 and 200 K-points, respectively, in the irreducible Brillouin Zone (IBZ) for our calculation. The BoltzTraP code [21] was used to calculate thermoelectric (TE) properties from ab-initio data using the semi-classical Boltzmann transport theory within the constant relaxation time and rigid band approximations.

3. Results and discussion

3.1. Electronic properties

It is interesting to note that ErN turns out to be a semiconductor for the majority spin based on the band structure shown Fig. 2. An indirect band gap at 0.79 eV, with the valence band maximum (VBM) can be seen at point Γ and the conduction band (CBM) at point X in the spin-orbit coupling effect with the Hubbard approach. On the other hand, the electronic band structure of $Er_{0.125}Ga_{0.875}N$ is shown in Fig. 3, the VBM is located at point K and CBM at point Γ of the Brillouin zone, which means that we have an indirect band gap at 3.38 eV using the GGA + U approach and a spin coupling effect, which is in good agreement with Filhol *et al*., [22] in wurtzite and in contrast with cubic structures found by Lantri *et al*. [23] and Lazreg *et al*. [24]. $Er_{0.125}Ga_{0.875}N$ is, consequently, considered as a semiconductor. The band gap values with different approaches are depicted in Table I.
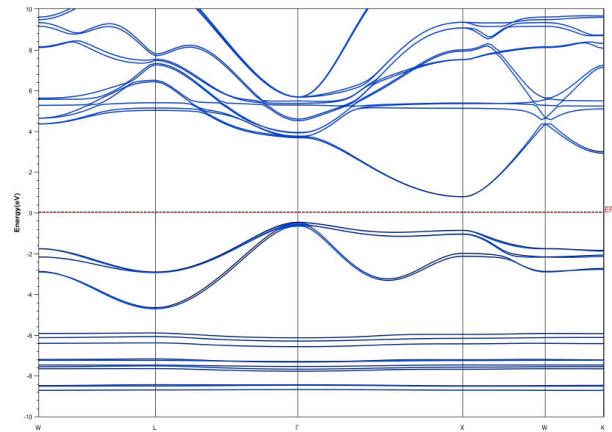

FIGURE 1. Unit cells of ErN and $Er_{0.125}Ga_{0.875}N$.
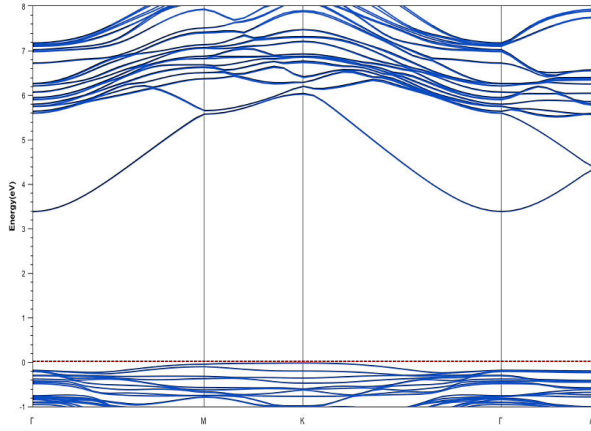

FIGURE 2. Band structure of ErN with GGAmbJ+U+so approximations.

FIGURE 3. Band structure of $Er_{0.125}Ga_{0.875}N$ with GGAmbJ+U+so approximations.

TABLE I. Band gap for ErN and $Er_{0.125}Ga_{0.875}N$ materials with different approximations.

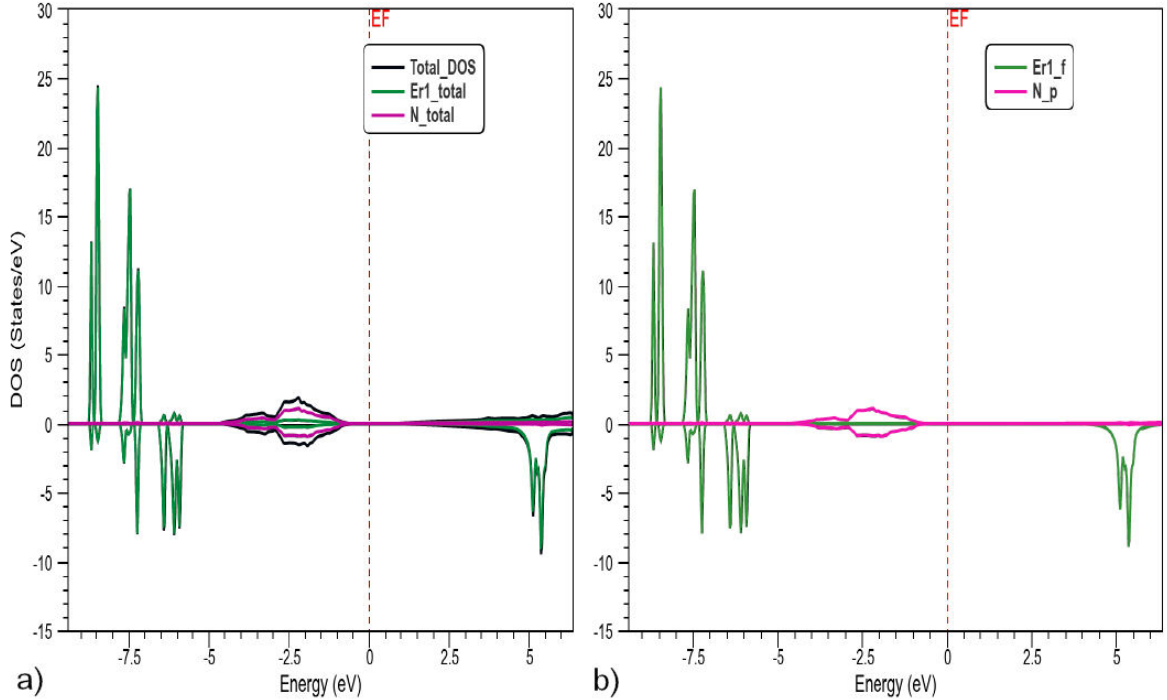| Materials	Approximation	Eg(eV)
ErN	GGA	0.000 (Metal)
	GGA+U	0.418
	mbJ +U+ so	0.790
	Other calculation	0.97 [25]
$Er_{0.06}Ga_{0.94}N$	GGA	0.666
	GGA+U	3.477
	mbJ+U+so	3.380
	Other calculation	3.109 [23]

FIGURE 4. Total and partial density of states of ErN with GGAmbJ+U+so approximations.

Total and partial spin polarized density of states of ErN are shown in Fig. 4. The valence bands are dominated by the $4f$ shell of Er states in the region ranging from -9 to -7.5 eV and by the $5p$ shell of N states from -3.5 to -1.5 eV. The bottom of the conduction band is dominated by $4f$ in range 4.5 to 5.5 eV. For the total DOS, the valence band is dominated by majority spin; in contrast, the conduction band is dominated by minority spin. The DOS of $Er_{0.125}Ga_{0.875}N$ is shown in Fig. 5, with the $4f$ shell of Er being dominant and the Ga $4p$ shell overlapping with the N $5p$ shell in the valence band. Conversely, the $4p$, $5p$ and $4f$ shell overlap in the conduction band.

3.2. Optical properties

The dielectric function describes the linear response of a material to a certain electromagnetic radiation wavelength or photon energy, which relates to the interaction of photons with electrons. Other optical properties can be derived from the complex dielectric function [26]. The following study is carried out using the formalism of Ehrenreich and Cohen, where the complex dielectric function can be written as

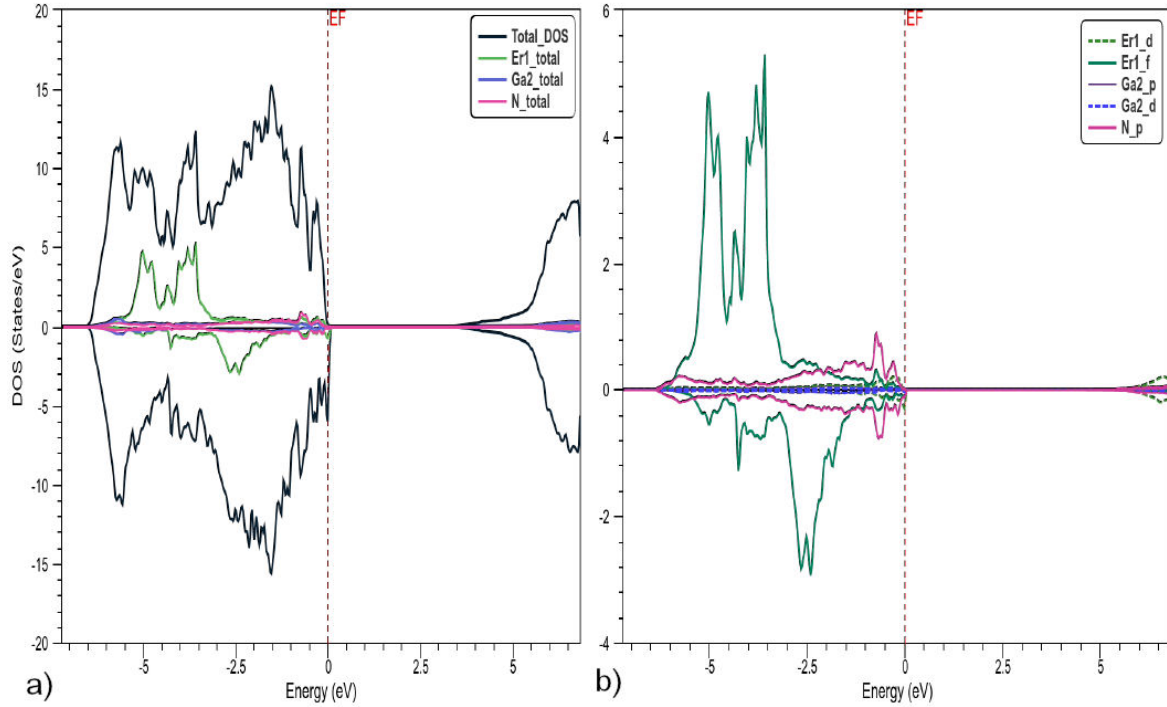$$\epsilon_r(\omega) = \epsilon'_r(\omega) + i\epsilon''_r(\omega), \qquad (1)$$

FIGURE 5. Partial density of states of $Er_{0.125}Ga_{0.875}N$ with GGAmbJ+U+so approximations.

$$\epsilon'_r(\omega) = 1 + \frac{2}{\pi} P \int_0^\infty \frac{\omega' \epsilon''_r(\omega')}{\omega'^2 - \omega^2} d\omega', \qquad (2)$$

$$\epsilon''_r(\omega) = \frac{2\omega}{\pi} P \int_0^\infty \frac{\epsilon'_r(\omega')}{\omega'^2 - \omega^2} d\omega', \qquad (3)$$

where ω is the integration variable, P represents the Chauchy principal value of the integral. Similarly, one can relate the real and imaginary parts of the polarizability, namely,

$$n(\omega) = 1 + \frac{2}{\pi} P \int_0^\infty \frac{K(\omega')}{\omega' - \omega} d\omega', \qquad (4)$$

and

$$K(\omega) = \frac{2}{\pi} P \int_0^\infty \frac{K(\omega')}{\omega' - \omega} d\omega'. \qquad (5)$$

The absorption coefficient $\alpha(E)$ is given by

$$\alpha(E) = \frac{4\pi}{\lambda} K(E), \qquad (6)$$

where λ is the wavelength of light in vacuum.The real part of the optical conductivity is calculated according to the following relation:

$$\sigma(\omega) = \frac{\omega}{4\pi} \epsilon(\omega). \qquad (7)$$

The most important property of a quantum well (QW) is the absorption coefficient, which can be written as

$$\alpha(\omega) = \frac{e^2 m^*}{2\epsilon_0 \epsilon_r c n_r \hbar L m_0^2} \frac{P^2}{\hbar\omega} \sum_{n,m} \langle g_v^m | g_c^n \rangle \Theta(E_{mn} - \hbar\omega), \quad (8)$$

where $\sum_{n,m} \langle g_v^m | g_c^n \rangle$ is the overlap integral between the z-dependent envelope functions of a conduction band and valence band, L is the width of quantum well, Θ is the Heaviside step function, n_r is the refractive index of the well material, and P is defined as $P = N \int_{cell} \psi^*_{k_c}(\vec{r}) p_A \psi_{k_v(\vec{r})} d^3 r'$. For a quantum well, $\chi_n(z) = \sqrt{2/L} \sin(n\pi z/L)$, and Eq. (8) can be recast in the form

$$\alpha(\omega) = \frac{2\pi e^2 \hbar}{\epsilon_0 \epsilon_r c n_r m^{*2} V} \frac{1}{\hbar\omega}$$
$$\times \sum_{i,j} |\langle i | p_z | j \rangle^2 | \delta(E_j - E_i - \hbar\omega)(f_{FD}^i - f_{FD}^j), \quad (9)$$

where i and j are the initial and final states and f_{FD} is the Fermi-Dirac distribution function. For two consecutive states, Eq. (9) may be written as:

$$\alpha(\omega) = \frac{2\pi e^2 \hbar}{\epsilon_0 \epsilon_r c n_r m^{*2} V} \frac{1}{\hbar} \left(\frac{8\hbar}{3L} \right)^2$$
$$\times \sum_{i,j} \delta(E_j - E_i - \hbar\omega)(f_{FD}^i - f_{FD}^j), \quad (10)$$

and Eq. (10) can be put into the from

$$\alpha(\omega) = \frac{n_s \pi e^2 \hbar}{2\epsilon_0 \epsilon_r c n_r m^* L} f_{21} \delta(\Delta E - \hbar\omega). \qquad (11)$$
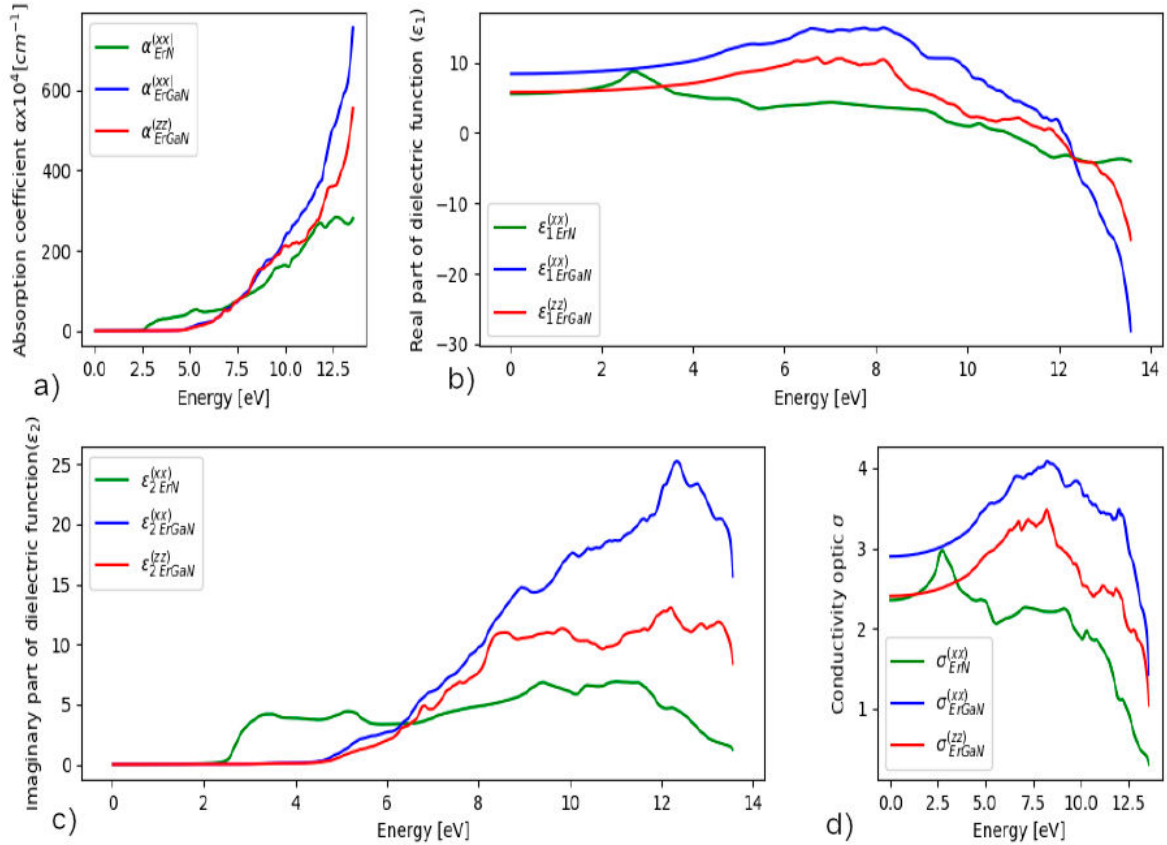
FIGURE 6. Optical properties: a) absorption coefficient, b) Real part(ϵ_1), c) Imaginary part (ϵ_2) of dielectric functions and d) optical conductivity (σ_{oc}) of ErN and $Er_{0.125}Ga_{0.875}N$ materials.

Here n_s is sheet charge density and f_{21} defines oscillator strength from the first to the second state. The total absorption coefficient of QW is the sum of confined states α_w and free states continuum α_b approximated by the barrier absorption coefficient given as follows [27,28]:

$$\alpha_{Tot} = \alpha_w(\omega) + \alpha_b(\omega). \tag{12}$$

This parameter is calculated by combining two numerical techniques; the first describes the optical properties for both materials (ErN, $Er_{0.125}Ga_{0.875}N$) using the Wien2k package with GGAmBj+ U including a spin-orbit coupling effect, and the second consists in optical properties of QW [27,29]. Figure 6a) shows the results of the absorbtion coefficient; we noted increasing absorption trends of ErN and $Er_{0.125}Ga_{0.875}N$ while changes in absorption during energy range 0-14 eV. For ErN, the absorption begins at a slightly lower energy, 0.8 eV (1550 nm). It is worth noting that absorption for $Er_{0.125}Ga_{0.875}N$ begins at 3.4 eV (365 nm), which covers a large portion of the solar spectrum. The variation of the optical conductivity is shown in Fig. 6d), where begins to increase and arrives at a maximum of at 2 eV for ErN and 8 eV in $Er_{0.125}Ga_{0.875}N$ for both (xx) and (zz) directions. The evolution of the refractive index and extinction coefficient are shown in Fig. 7. We note that the static refractive index of
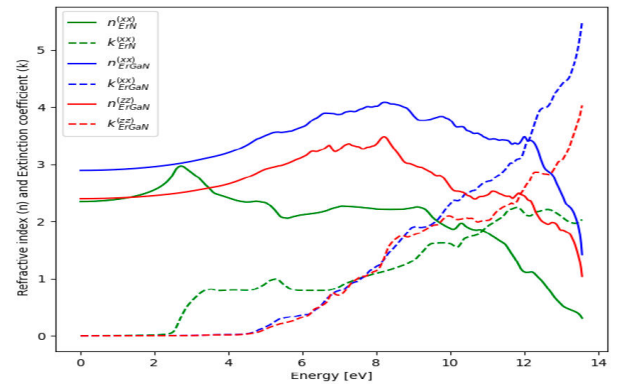

FIGURE 7. Index refraction and extinction coefficient of ErN and $Er_{0.125}Ga_{0.875}N$ materials.

ErN is 2.3; it begins to increase until reaches its maximum at 2.8 and for $Er_{0.125}Ga_{0.875}N$, the static refractive indices are 2.9 and 2.4, it shows an increase until it reaches its maximum at 4 and 3.4 for (xx) and (zz) directions. Thus, the extinction coefficient starts to increase from a threshold equal to 2.6 eV for ErN and 3.0 eV for ErGaN in (xx) and (zz) directions.
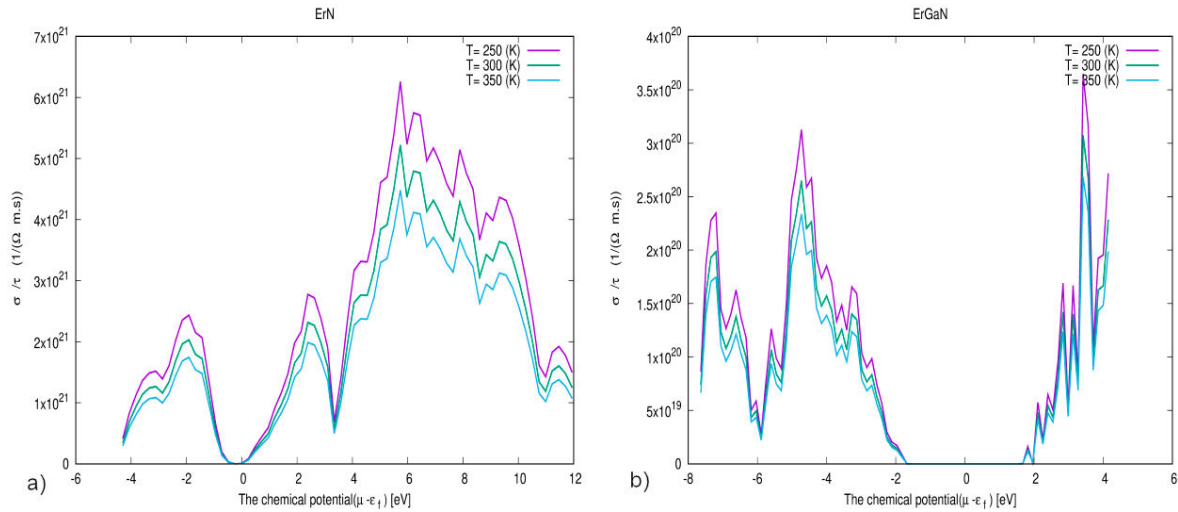
FIGURE 8. Electrical conductivity of ErN and $Er_{0.125}Ga_{0.875}N$ at three constant temperatures.
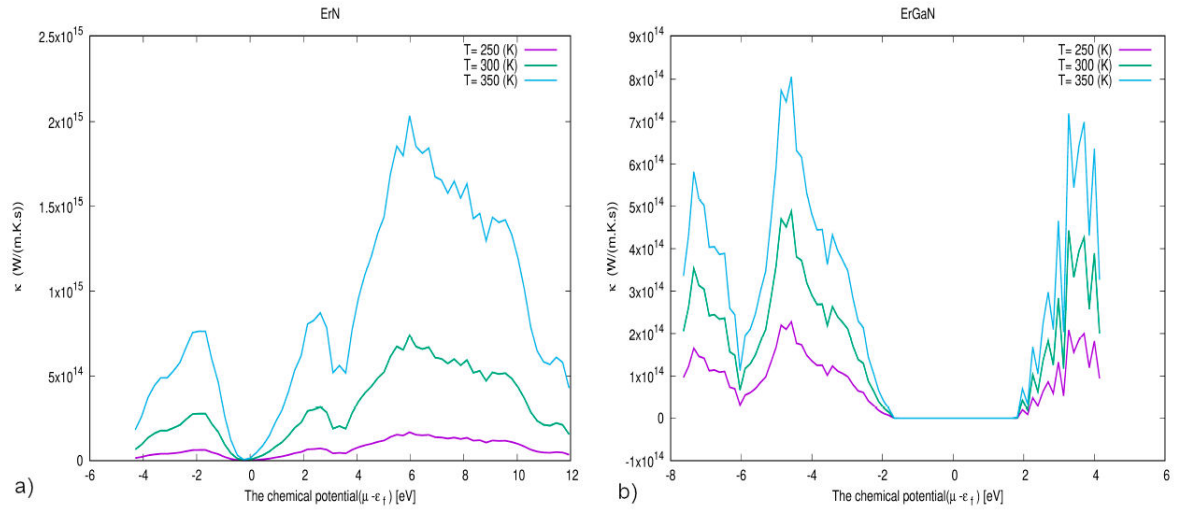

FIGURE 9. Electronic thermal conductivity of ErN and $Er_{0.125}Ga_{0.875}N$ at three constant temperatures.

3.3. Transport properties

The effectiveness of a material for TE applications is determined by the dimensionless figure of merit, $ZT = \sigma S^2 T/\kappa$, where S is the Seebeck coefficient, σ is the electrical conductivity, T is the absolute temperature, and κ is the thermal conductivity. High values of figure of merit require high values of S and σ and low value of κ. The power factor of a TE material is given by $P = \sigma S^2$, which involves all the important electrical properties of the material. Our calculations of TE for ErGaN/ErN are performed separately on bulk materials, using the BoltzTrap code [21].

The electrical conductivity as a function of chemical potential at three constant temperatures (250,300,350) K is shown in Fig. 8, where it is clear that (σ/τ) of ErN and ErGaN increases as temperature decreases. The maximum electrical conductivity (σ/τ) of ErN and ErGaN was found to be 6.2×10^{21} 1/Ωms and 3.7×10^{20} 1/Ωms at 5.3 eV and 3.5 eV, respectively, at 250 K. The electronic thermal conductivity (κ) as a function of chemical potential is plotted in Fig. 9, and it shows clearly that κ for ErN and ErGaN increases as temperature rises. The Seebeck coefficient as a function of chemical potential at (250,300,350)K is shown in Fig. 10. Its maximum values were found to be 530 μV/K (at 250 K) and 1400 μV/K (at 300 K) respectively. In Fig. 11 shows the electronic power factor (PF) calculated as a function of chemical potential at three constant temperatures. Our calculated show that ErN has its the highest power factor with a value of 6×10^9 W/mK^{2}s at 350 K and energy level of ErN is 9×10^{10} W/mK^{2}s at 350 K and energy level of 2 eV. The electronic power factor is a keynote quantity for measuring transport properties.

4. Conclusion

We have studied materials involved in constructing QW of $Er_{0.125}Ga_{0.875}N$/ErN by ab-initio calculation using DFT theory. The obtained results of the electronic properties show clearly ErN to be a semiconductor with an indirect band gap at 0.79 eV and that $Er_{0.125}Ga_{0.875}N$ presents an indirect band gap at 3.38 eV, using GGA+U approaches, which is in good agreement with other calculations. This indirect band gap was found to improve carrier extractions and lead to improved performance of these properties. The real and imaginary parts of the dielectric function and the optical coefficients were determined. Transport properties of $Er_{0.125}Ga_{0.875}N$ and ErN have been investigated by employing the Boltzman theory implemented in the BoltzTrap code, the electrical conductivity, Seebek coefficient, electronic thermal conductivity, and electronic power factor have been determined; their values show that these materials could be potential candidates for energy conversion. The quantized energy levels present in a quantum well, which can be tuned, provide an opportunity to increase the limited efficiency of solar cells.

1. L. C. Bannow *et al.*, An ab initio based approach to optical properties of semiconductor heterostructures, *Model. Simul. Mater. Sci. Eng.* **25** (2017) 065001, https://doi.org/10.1088/1361-651X/aa7478.

2. R. Dahal, C. Ugolini, J. Y. Lin, H. X. Jiang, and J. M. Zavada, Erbiumdoped GaN optical amplifiers operating at 1.54 μm, *Appl. Phys. Lett.* **95** (2009) 111109, https://doi.org/10.1063/1.3224203.

3. S. Tab *et al.*, Structural, elastic, electronic, and magnetic properties of quaternary alloys $BBi_{0.75}Mn_{0.125}N_{0.125}$: A first-principles study, *Rev. Mex. Fis.* **66** (2020) 627, https://doi.org/10.31349/RevMexFis.66.627.

4. B. Amiri, A. Lazreg, and F. A. Bensamer, Optical and Thermoelectric properties of Gd doped Wurtzite GaN, *Optik* **240** (2021) 166798, https://doi.org/10.1016/j.ijleo.2021.166798.

5. A. G. Petukhov, W. R. L. Lambrecht, and B. Segall, Electronic structure of rar-earth pnictides, *Phys. Rev. B* **53** (1996) 4324, https://doi.org/10.1103/PhysRevB.53.4324.

6. K. P. O'Donnell and V. Dierolf, Rare Earth Doped III-Nitrides for Optoelectronic and Spintronic Applications (Springer, Dordrecht, 2010), https://doi.org/10.1007/978-90-481-2877-8.

7. C. Ugolini *et al.*, Formation energy of optically active Er^{3+} centers in Er doped GaN, *Appl. Phys. Lett.* **101** (2012) 051114, https://doi.org/10.1063/1.4742196.

8. S. Kasap and P. Capper, Nano-Engineered Tunable Photonic Crystals, in Springer Handbook of Electronic and Photonic Materials (Springer, Cham, 2017), https://doi.org/10.1007/978-3-319-48933-9.

9. T. Trupke, M. A. Green, and P. Würfel, Improving solar cell efficiencies by up-conversion of sub-band-gap light, *J. Appl. Phys.* **92** (2002) 4117, https://doi.org/10.1063/1.1505677.

10. M. Haase and H. Schäfer, Upconverting Nanoparticles, *Angew. Chem. Int. Ed.* **50** (2011) 5808, https://doi.org/10.1002/anie.201005159.

11. M. B. Spitzer, H. P. Jenssen, A. Cassanho, An approach to downconversion solar cells, *Sol. Energy Mater. Sol. Cells* **108** (2013) 241, https://doi.org/10.1016/j.solmat.2012.08.011.

12. A. J. Steckl, J. H. Park, and J. M. Zavada, Prospects for rare earth doped GaN lasers on Si, *Mater. Today* **10** (2007) 20, https://doi.org/10.1016/S1369-7021(07)70176-1.

13. T. M. Al Tahtamouni, M. Stachowicz, J. Li, J. Y. Lin, and H. X. Jiang, Dramatic enhancement of 1.54 μm emission in Er doped GaN quantum well structures, *Appl. Phys. Lett.* **106** (2015) 121106, https://doi.org/10.1063/1.4916393.

14. W. Kohn, Density Functional and Density Matrix Method Scaling Linearly with the Number of Atoms, *Phys. Rev. Lett.* **76** (1996) 3168, https://doi.org/10.1103/PhysRevLett.76.3168.

15. W. Kohn and L. J. Sham, Self-Consistent Equations Including Exchange and Correlation Effects, *Phys. Rev.* **140** (1965) A1133, https://doi.org/10.1103/PhysRev.140.A1133.

16. P. Blaha *et al.*, WIEN2k: An Augmented Plane Wave Plus Local Orbitals Program for Calculating Crystal Properties, 2001.

17. E. Sjöstedt, L. Nordström, and D. J. Singh, An alternative way of linearizing the augmented plane-wave method, *Solid State Commun.* **114** (2000) 15, https://doi.org/10.1016/S0038-1098(99)00577-3.

18. K. Schwarz and P. Blaha, Solid state calculations using WIEN2k, *Comput. Mater. Sci.* **28** (2003) 259, https://doi.org/10.1016/S0927-0256(03)00112-5.

19. B. N. Harmon, V. P. Antropov, A. I. Liechtenstein, I. V. Solovyev, and V. I. Anisimov, Calculation of magneto-optical properties for $4f$ systems: LSDA + Hubbard U results, *J. Phys. Chem. Solids* **56** (1995) 1521, https://doi.org/10.1016/0022-3697(95)00122-0.

20. F. Tran and P. Blaha, Accurate Band Gaps of Semiconductors and Insulators with a Semilocal Exchange-Correlation Potential, *Phys. Rev. Lett.* **102** (2009) 226401, https://doi.org/10.1103/PhysRevLett.102.226401.

21. G. K. H. Madsen, J. Carrete, and M. J. Verstraete, BoltzTraP2, a program for interpolating band structures and calculating semi-classical transport coefficients, *Comput. Phys. Commun.* **231** (2018) 140, https://doi.org/10.1016/j.cpc.2018.05.010.

22. J.-S. Filhol, R. Jones, M. J. Shaw, and P. R. Briddon, Structure and electrical activity of rare-earth dopants in GaN, *Appl. Phys. Lett.* **84** (2004) 2841, `https://doi.org/10.1063/1.1710710`.

23. M. Lantri *et al*., Effect of Erbium doping on GaN electronic and optical properties: First-principles study, *Mod. Phys. Lett. B* **33** (2019) 1950327, `https://doi.org/10.1142/S0217984919503275`.

24. A. Lazreg, Z. Dridi, F. Benkabou, and B. Bouhafs, Electronic structure of cubic $Er_xGa_{1-x}N$ using the LSDA+U approach, *Phys. B* **403** (2008) 2702, `https://doi.org/10.1016/j.physb.2008.02.003`.

25. P. Larson, W. R. L. Lambrecht, A. Chantis, and M. van Schilfgaarde, Electronic structure of rare-earth nitrides using the LSDA+U approach: Importance of allowing $4f$ orbitals to break the cubic crystal symmetry, *Phys. Rev. B* **75** (2007) 045114, `https://doi.org/10.1103/PhysRevB.75.045114`.

26. J. Singh, Optical Properties of Condensed Matter and Applications (John Wiley and Sons, New York, 2006), `https://doi.org/10.1002/0470021942`.

27. B. Amiri, A. Belghachi, H. Benslimane, and A. Talhi, Potential of multiplequantum well tandem solar cells based on $GaP_xAs_{1-x}/Ga_yIn_{1-y}As$, *Optik* **147** (2017) 283, `https://doi.org/10.1016/j.ijleo.2017.08.081`.

28. S. Fara, P. Sterian, L. Fara, M. Iancu, and A. Sterian, New Results in Optical Modelling of Quantum Well Solar Cells, *Int. J. Photoenergy* **2012** (2012) 810801, `https://doi.org/10.1155/2012/810801`.

29. P. Harrison and A. Valavanis, Quantum Wells, Wires and Dots: Theoretical and Computational Physics of Semiconductor Nanostructures, 4th ed. (Wiley, New York, 2016).